Thermomechanical Analysis in Electronic Packaging with Unified Constitutive Model for Materials and Joints

Chandra S. Desai, Cemalettin Basaran, Terrance Dishongh, and John L. Prince, *Fellow, IEEE*

***Abstract*— A unified constitutive modeling approach based on the disturbed state concept (DSC) provides improved characterization of thermomechanical response of joining (solders), ceramics and printed wire board (PWB) materials in electronic packaging. Various versions in the DSC approach are calibrated and validated with respect to laboratory test data, and are implemented in a nonlinear finite element (FE) procedure. The hierarchical nature of this procedure permits the user to choose a constitutive model, simple (elastic) to sophisticated (elastoviscoplastic with disturbance), depending upon the material and need. The FE is used to analyze thermomechanical behavior of two typical problems:**

1) leadless ceramic chip carrier (LCCC) package;
2) solder ball connect (SBC) package.

The FE results under cyclic thermal loading are compared with experimental data for the two packages, and with a previous FE analysis for the SBC package. In conjunction with the idea of critical disturbance at which thermal fatigue failure can occur, the analyzes allow identification of cycles to failure, N_f, and evaluation of reliability of the package. In the case of the SBC package, the analysis permits an evaluation of ball spacing on the thermomechanical behavior.

The DSC approach can provide an integrated and improved procedure compared to available models for elastic, plastic, creep strains, and microcracking leading to degradation of strength and fatigue failure for a wide range of problems in electronic packaging under thermomechanical loading.

***Index Terms*— Calibration, chip-substrate systems, electronic packaging, finite element analysis, materials and joints, reliability, thermomechanical behavior, unified constitutive model, validation.**

I. Introduction

Appropriate characterization of the thermomechanical behavior of materials and interfaces or joints plays a vital role in the realistic and economical design in electronic packaging such as chip-substrate systems. Although significant experimental, analytical and computational research has been reported, see reviews in [1]–[7], there appears to be a lack of unified and fundamental constitutive models that can be implemented readily in numerical procedures for improved and economical analysis, design and reliability.

The research conducted toward the goal of developing realistic models and computer analysis has involved:

1) development of a unified constitutive model based on the newly proposed disturbed state concept (DSC) to characterize the behavior of materials in the joints/interfaces, chips and substrates;
2) calibration of the model parameters based on available laboratory tests, particularly on Pb-Sn solder materials;
3) use of available test data and development of new laboratory test devices for enhanced databases for material parameters;
4) validation of the model using the laboratory test data;
5) implementation of the model in numerical finite element procedures with application to and validation of practical chip-substrate problems in electronic packaging.

Details of the first three aspects are presented in various publications [6]–[8], hence, a brief review is given below. The main attention here is given to the fourth aspect, namely, thermomechanical analysis including failure and reliability of two typical problems in electronic packaging.

II. Constitutive Model

A general and unified constitutive model based on the disturbed state concept (DSC) [9], [10] has been developed to account for elastic, plastic and creep strains, microcracking, damage and degradation or softening, and post-peak stiffening under thermomechanical loading for a number of materials used in electronics industry. The hierarchical nature of this approach provides the user the flexibility to choose an appropriate model for a specific need. For instance, one can choose elastic, classical elastoplastic, thermoelastic, thermoviscoplastic, to the general model, thermoviscoplastic with disturbance, which includes the classical damage model as a special case. As a result, the DSC provides improved and integrated modeling of joining and chip-substrate materials, compared to those available in the past.

The Disturbed State Concept: The disturbed state concept (DSC) is based on the consideration that at any stage during thermomechanical loading, a material element is composed of the materials in two component states: relative intact (RI) and fully adjusted (FA) (Fig. 1). Initially, before the application of the load, the material is either in complete RI state, or with

Manuscript received November 25, 1996; revised October 29, 1997. This work was supported by Grants DDM-9 102 177 and DMI-9 313 204 from the National Science Foundation, Washington, DC, Manufacturing and Mechanics Divisions.

C. S. Desai and J. L. Prince are with The University of Arizona, Tucson, AZ 85721 USA.

C. Basaran is with the State University of New York, Buffalo, NY 14260 USA.

T. Dishongh is with Intel Corporation, Hillsboro, OR 97124 USA.

Publisher Item Identifier S 1070-9894(98)01029-9.

1070–9894/98$10.00 © 1998 IEEE

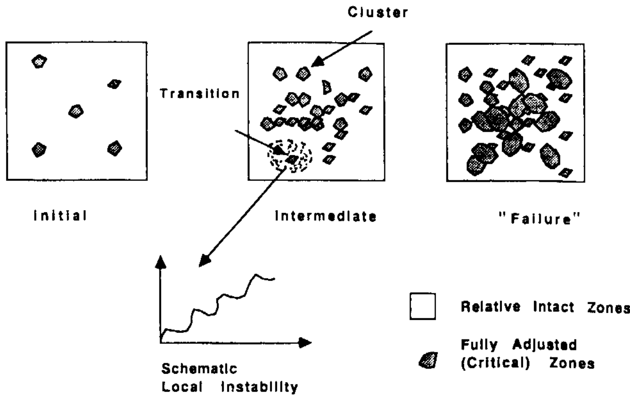

Fig. 1. Schematic of relative intact and fully adjusted clusters in DSC.

a (small) part in the FA state, representing cracks or flaws due to initial effects such as residual stress and manufacturing. As the loading progresses, the material experiences continuous changes or disturbances in its microstructure due to the process of natural self-adjustment of its particles. As a consequence, the RI state transforms to the FA state; they are distributed randomly, Fig. 1. In the limit, the entire material element approaches asymptotically the FA state. Somewhere before the final FA state, the microstructure reaches a critical combination of the RI and FA states, which can be identified as the critical disturbance, at which it "fails," or *collapses*, and ceases to perform its engineering service function. Evaluation of this failure state under cyclic thermal loading is important for reliability analysis of packaging problems.

The observed response is expressed in terms of the responses in the RI and FA states by using the disturbance function, D. The response of the material in the RI state can be found from laboratory stress-strain-volume change and/or nondestructive behavior, and can be characterized by using such continuum theories as elasticity, plasticity, thermoplasticity and thermoviscoplasticity [6]–[10].

In the FA state, the material behaves differently compared to the RI material, and its response is usually much softer. As it is surrounded by the RI material, it does possess certain strength, however. For instance, for a given initial mean pressure, it can continue to carry the shear stress reached up to that state and deform in shear at constant volume; this state is often termed as the critical state. Thus, in contrast to the classical continuum damage models [11] in which the damaged material part has no strength, the FA material in the DSC possesses finite strength. One of the attributes of this approach is that the observed material response involves consideration of responses of two coupled and interacting material parts, and as a consequence, the microcrack interaction effects are implicitly accounted for in the DSC model [9], [10].

Disturbance Function: The disturbance function denotes the proportion of the volume of material parts in the FA state to the total volume of the material elements, and acts as the coupling and interpolation mechanism between the RI and FA responses so as to lead to the observed response. It is expressed as a function of such internal variables as the viscoplastic strain trajectory, temperature and cyclic loading, and is calibrated from laboratory test data. It is often expressed as

$$D = D_u\left(1 - e^{-A\xi_D^Z}\right) \tag{1}$$

where D_u, A and Z can be temperature (θ) dependent material parameters and ξ_D is given by

$$\xi_D = \int \left(d\epsilon_{ij}^{\mathrm{vp}\theta} \quad d\epsilon_{ij}^{\mathrm{vp}\theta}\right)^{1/2} \tag{2}$$

where $\epsilon_{ij}^{\mathrm{vp}\theta}$ is the tensor of thermoviscoplastic deviatoric strains, ξ_D is their trajectory, and d denotes increment. The parameters A, Z, and D_u are found from laboratory tests in terms of stress-strain, volumetric and/or nondestructive responses. Accordingly, D can be expressed as (10)

$$D_\sigma = \frac{\sqrt{J_{2D}^i} - \sqrt{J_{2D}^a}}{\sqrt{J_{2D}^i} - \sqrt{J_{2D}^c}} \tag{3a}$$

$$D_v = \frac{v^i - v^a}{v^i - v^c} \tag{3b}$$

$$D_n = \frac{V^i - V^a}{V^i - V^c} \tag{3c}$$

where J_{2D} is the second invariant of the deviatoric stress, S_{ij}, and is proportional to shear stress, τ, v is the volume, V is the ultrasonic velocity, and a, i and c denote observed, RI and FA states, respectively.

Constitutive Equations: Based on equilibrium of forces in, observed, RI, and FA parts in the material element, the incremental constitutive equations are derived as [6]–[10]

$$d\sigma_{ij}^a = (1 - D)C_{ijkl}^i d\epsilon_{kl}^i + DC_{ijkl}^c d\epsilon_{kl}^i + dD\left(\sigma_{ij}^c - \sigma_{ij}^i\right) \tag{4}$$

where σ_{ij} is the stress tensor, C_{ijkl}^i and C_{ijkl}^c are the constitutive tensors that characterize the RI and FA parts, respectively, and dD is the increment or rate of D. As indicated earlier, the RI behavior can be characterized by using appropriate continuum theory such as elasticity, elastoplasticity and viscoplasticity.

The FA behavior can be characterized by using the critical state concept or by assuming that the material part in that state can carry no shear stress but can carry hydrostatic state [6], [7], [12]. The latter is used for joining materials such as solder alloys here. It implies that the material parts in the FA state, surrounded by material parts in the RI state, act like a *constrained liquid*; this is analogous to the plastic state after the yield in perfect plasticity. In this case, the tensor C_{ijkl}^c involves the parameters related to the volumetric or bulk behavior.

III. Material Parameters

As indicated earlier, the user can choose a model for a specific need. Various (12) options available are given in Table I. The material parameters are found from available laboratory tests. Here, the parameters for various solders are found from tests reported previously [13]–[19]; procedures for finding the parameters are given in [6]–[8]. It may be noted that the parameters in the DSC model have physical meanings and are related to strategic states during deformation behavior of

TABLE I
VARIOUS OPTIONS IN THE DSC AND PARAMETERS

Model	Parameters		Creep	Disturbance	Thermal Effects (θ)*
	Elastic	Plastic			
1. Elastic (E)	E, ν				2. E(θ)
3. Elastic-plastic classical (EP/C), e.g., von Mises	E, ν	σ_y			4. EP/C(θ)
5. Elastic-plastic hardening (EP/H)	E, ν	γ, β; n; a_1, η_1			6. EP/H(θ)
7. EP/H with disturbance	E, ν	γ, β; n; a_1, η_1		A, Z, D_u	8. EPH(θ) with disturbance
9. Elastic viscoplastic (EVP)	E, ν	γ, β; n; a_1, η_1	Γ, N		10. EVP(θ)
11. Elastic viscoplastic (EVP) with disturbance	E, ν	γ, β; n; a_1, η_1	Γ, N	A, Z, D_u	12. EVP(θ) with disturbance

*Thermal effects are included by expressing the parameters as in Eq. (5).
σ_y = yield stress

materials. The following equation defines the temperature-dependent parameters shown in Table I; the meanings of various parameters (in Table I) are given subsequently

$$p = p_{300}\left(\frac{\theta}{300}\right)^{\lambda} \tag{5}$$

where p is a parameter, p_{300} is the value of p at 300 K, θ is the temperature, and λ is the exponent. Hence, p_{300} and λ need to be determined from laboratory tests.

The strain rate ($\dot{\epsilon}$) effects need to be included for characterizing the materials. It is possible to express the parameters as function of $\dot{\epsilon}$ [6]; this aspect is beyond the scope of this paper. Here, average values are used if more than one test for strain rates were available.

Validation: The parameters were used to backpredict the laboratory test data for various solders by integrating (4). Here, the validations were obtained for the tests used to find the parameters and independent tests not used to find them. Details are given by [6]–[8].

Meanings of Parameters: Various parameters in Table I are defined below.

Elastic. Young modulus E and Poisson's ratio, ν, or shear modulus, G, and bulk modulus, K, are found from unloading or initial slopes of observed stress-strain curves.

Plasticity. The yield function in the HISS plasticity approach is given by [6]

$$F = J_{2D} - \left[-\alpha\bar{J}_1^n + \gamma\bar{J}_1^2\right](1-\beta S_r)^{-0.5} = 0 \tag{6a}$$

where γ and β can be temperature dependent and are related to the ultimate or failure envelope in the $\sqrt{J_{2D}} - J_1$ stress space, n is the phase change parameter and denotes the states at which the volume change is zero, $S_r = \sqrt{27}/2 J_{2D} \cdot J_1^{-1.5}$, J_1 is the first invariant of stress tensor σ_{ij}, J_{2D} and J_{3D} are the second and third invariants of S_{ij}; here, the

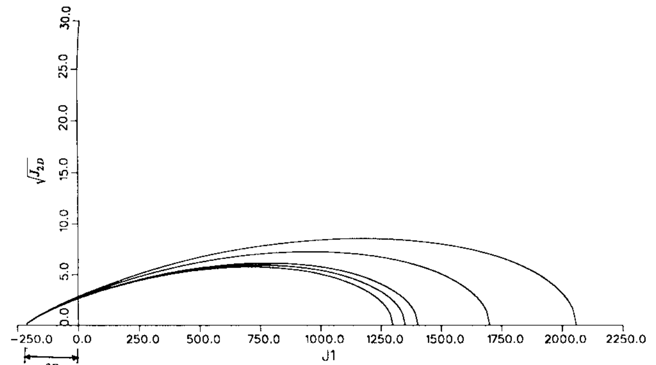

Fig. 2. Schematic of yield function with bonding stress.

stress quantities are nondimensionalized with respect to the atmospheric pressure constant p_a so as to render most of the parameters nondimensional. The term $\bar{J}_1$ is given by

$$\bar{J}_1 = J_1 + 3R \tag{6b}$$

where R is the bonding stress. Fig. 2 shows schematic of yield function F with continuously expanding yield surfaces. The ultimate or failure yield surface intersects the J_1-axis at the value of $J_1 = 3R$ on the negative side.

The hardening or growth function, α, is given by

$$\alpha(\theta) = \frac{a_1(\theta)}{\xi_D^{\eta_1(\theta)}} \tag{7}$$

where a_1 and η_1 are temperature dependent hardening parameters.

Creep. The viscoplastic strain rate $\dot{\epsilon}_{ij}^{\mathrm{vp}\theta}$ given by [6], [20]

$$\dot{\epsilon}_{ij}^{\mathrm{vp}\theta} = \Gamma(\theta)\langle\psi(F)\rangle\frac{\partial F}{\partial\sigma_{ij}} \tag{8a}$$

where the flow function $\psi(F)$ is given by

$$\psi\left(\frac{F}{F_0}\right) = \begin{cases} 0, & \text{when } F \le 0 \\ \left(\frac{F}{F_0}\right)^{N(\theta)}, & \text{when } F > 0 \end{cases} \tag{8b}$$

Here, the fluidity parameter, Γ, and the exponent, N, can be temperature dependent, and F_0 is the normalizing function, e.g., yield stress in uniaxial tension or p_a.

Disturbance. The temperature dependent disturbance parameters A, Z and D_u are defined in (1). Details including values of these parameters are given later for the two example problems.

Validation. The DSC models have been validated with respect to laboratory test data for a wide range of solders, silicon and ceramic-composite [6]–[10].

IV. Finite Element Procedure

The DSC model (4) is implemented in a nonlinear finite element procedure that permits elastic, elastoplastic, elastoviscoplastic, thermo-elasticviscoplastic and disturbance versions. The finite element equations for the general thermoviscoplastic model with disturbance are shown below [7], [8]; note that these equations will be simplified for various options in Table I:

$$\begin{aligned} \sum_m \int_V [B]^T ((1-D)[^iC^{\text{evp}\theta}] \\ + D(1+\alpha^*)[^cC^{\text{evp}\theta}])[B]\{\Delta q^i\} \\ = \{Q\} - \sum_m \int_V [B]^T \{\sigma^a\}\, dV \\ - \sum_m \int [B]^T \{\sigma_n^c - \sigma_n^i\}\, dD\, dV \end{aligned} \tag{9}$$

where $[B]$ is the strain-displacement transformation matrix, α^* is the relative strain parameter in $\{d\epsilon^c\} = (1+\alpha^*)\,\{d\epsilon^i\}$, $\{\Delta q\}$ is the incremental nodal displacement vector, m is the number of elements, and superscript (evpθ) denotes thermo-elastoviscoplastic. For viscoplastic analysis, (9) is solved using time integration, while for other options, Table I, its special forms are solved using incremental-iterative techniques [6]–[8].

V. Applications

A. Design

The DSC provides a basis for developing design charts for given (class of) joining materials. Here, a typical chip-substrate system was subjected to cyclic shear strain cycles (N) of different amplitudes and temperatures. The results were obtained in terms of growth of disturbance, peak shear stress and load factor (ϕ) [18] with N. Based on an adopted criteria for fatigue failure, such as $D = 50\%, 75\%, 95\%$; it was possible to define the number of corresponding cycles at failure, N_f. Comprehensive parametric study involving variation of various parameters, can lead to nondimensionalized design charts for the evaluation of their fatigue life; details are given in [6].

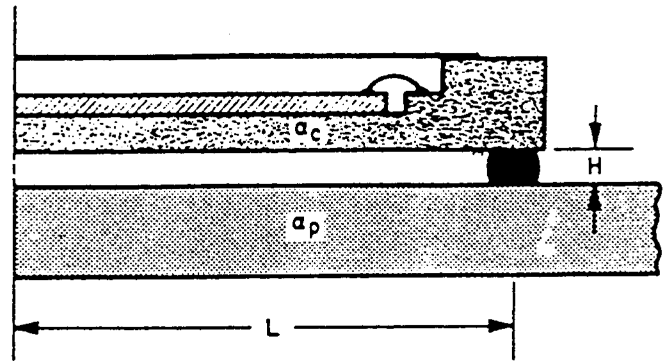

(a)

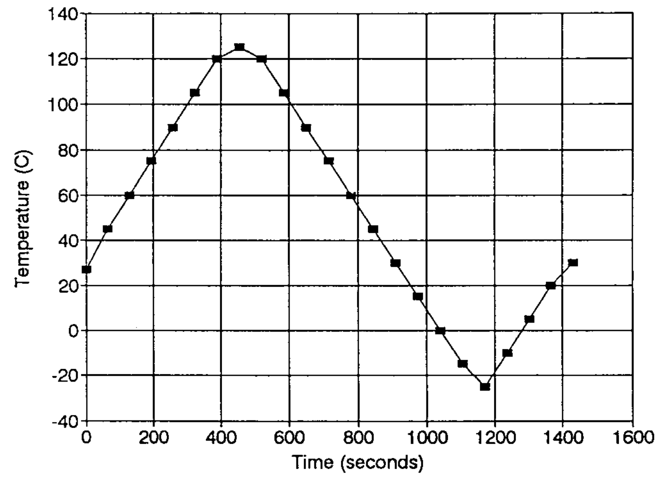

(b)

Fig. 3. Leadless ceramic chip carrier and temperature cycles [21]: (a) LCCC and (b) temperature cycle.

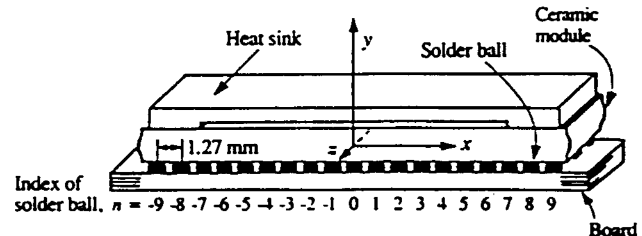

Fig. 4. Example 2: Test vehicle for CBGA in simulated laboratory test [24].

B. Examples in Electronic Packaging

A main objective here is to describe two typical problems in electronic packaging that have been solved by using the FE procedure with the DSC model. The first example involves laboratory tests performed by Hall and Sherry [21] on an 84 I/O, 0.64 mm pitch leadless ceramic chip carrier (LCCC) mounted on a printed wiring board (FR4, polymide epoxy glass) by using a (60% Sn-40% Pb) eutectic solder, Fig. 3(a). The material properties used are those obtained from the tests reported by Riemer [13] and Skipor, *et al.* [17] for elasto-plastic, Pan [16] for creep, and Solomon [18] for disturbance. They are listed in Table II with respect to their temperature dependence.

The second example represents analysis of IBM 604 power PC chip which involves *ceramic ball grid array* (CBGA) composed of either alumina or aluminum nitride (ALN) which

TABLE II
MATERIAL PARAMETERS FOR EXAMPLE 1: LCCC AND EXAMPLE 2: SBC

	Example 1: 60% Sn-40% Pb Solder		Example 2: SBC			
			63% Pb-37% Sn		90% Pb-10% Sn	
Parameter	p_{300}	λ	p_{300}	λ	p_{300}	λ
Elasticity						
E	23.0 GPa	-0.30	15.7 GPa	-4.1	9.29 GPa	-1.92
ν	0.40	0.14	0.40	0.0	0.40	0.0
Plasticity						
γ	0.00082	-0.034	0.00081	-0.158	0.000822	-0.16
a_1	2.4×10^{-5}	-2.58	0.78×10^{-5}	0.00	1.10×10^{-5}	-0.61
η_1	0.394	0.00	0.46	0.23	0.44	0.24
n	2.10	0.0	2.10	0.00	2.10	0.00
R	217.0 MPa	-2.95	208.0 MPa	-5.34	122.0 MPa	-1.67
Creep						
Γ	1.80/sec	6.20				
N	2.67	0.00				
Disturbance						
A	0.102	1.55	0.102	1.55	4.07	0.00
Z	0.676	0.00	0.676	0.0	1.95	0.00
D_u	1.00	---	0.90	0.0	0.90	0.00

Chip and PWB: Elastic

Chip		Ceramic Module	
E	255.0 GPa	E	318.0 GPA*
ν	0.30	ν	0.23
α_T	$5.4 \times 10^{-6}/°C$	α_T	$7.0 \times 10^{-6}/°C$
PWB		**PWB (FR-4)**	
E	12.0 GPa	E	11.0 GPa
ν	0.36	ν	0.28
α_T	$8.9 \times 10^{-6}/°C$	α_T	$20 \times 10^{-6}/°C$

α_T—Co-efficient of thermal expansion. *From special laboratory tests [8].

encases a controlled collapsible chip connection (C-4) silicon chip; details of geometry and dimensions are given in (22, 23). Details of the CBGA in simulated laboratory test used later for comparison are shown in Fig. 4. Here, the material parameters are determined from tests reported by Cole *et al.* [15] and Savage and Getzan [19] for elastoplastic, and Nir *et al.* [14] for disturbance. These parameters for different materials are listed in Table II.

The solder (60% Sn-40% Pb) in Example 1 is characterized as thermoelastoviscoplastic with disturbance, and for Example 2, the two solders, (63% Sn-37% Pb) and (90% Pb-10% Sn), are characterized as elastothermoplastic with disturbance. The material in the chip and PWB are assumed to be linear elastic. In the case of aluminum nitride (ALN) substrate, a series of tension and compression tests were performed [8] to determine its elastic constants.

Example 1: Leadless Ceramic Chip Carrier (LCCC) Package: Fig. 5(a) shows the finite element mesh for the problem in Fig. 3. The mesh for the solder is shown in Fig. 5(b). The chip-substrate system is subjected to thermal loading cycle, Fig. 3(b), as it was done in the laboratory tests. The FE analysis involved application of 2000 thermal cycles. The analysis was performed in two stages. In the first stage, the entire mesh [Fig. 5(a)] was used and one thermal cycle (N) was applied, which resulted in differential strains due to the thermal expansion mismatch (CTE). The net or relative displacements were identified in the solder, and were then applied at the top of the solder, Fig. 5(b), for 2000 thermal cycles, in the second stage. This macro (stage 1) and micro (stage 2) procedure is used to reduce computational effort.

Displacements, stresses, strains and disturbance (D) were computed during and after each thermal cycle. Fig. 6(a)–(c) shows distribution of disturbance at typical cycles $N = 100$, 300, and 400 cycles. Note that the disturbance represents the effect of accumulated plastic strains (2). It can be seen that the disturbance changes (increases) with N, starts to localize near the top right corner, and the localization grows from that corner through the solder toward the top left corner. This trend is similar to laboratory observations [21]. When a specific critical disturbance, $D_c \simeq 0.8$ to 0.90, covers a majority (about 90% of the area) solder, it can be considered to have failed from the viewpoint of its engineering service function. Such failure occurs around 350 cycles [Fig. 6(b) and (c)]. Hall and Sherry [21] reported that the laboratory test specimen failed after about 346 thermal cycles. Thus, the computed cycles at failure, N_f, compare well with those observed in the laboratory.

The idea of the critical disturbance, D_c, to define failure, can have significant potential for design and reliability analysis.

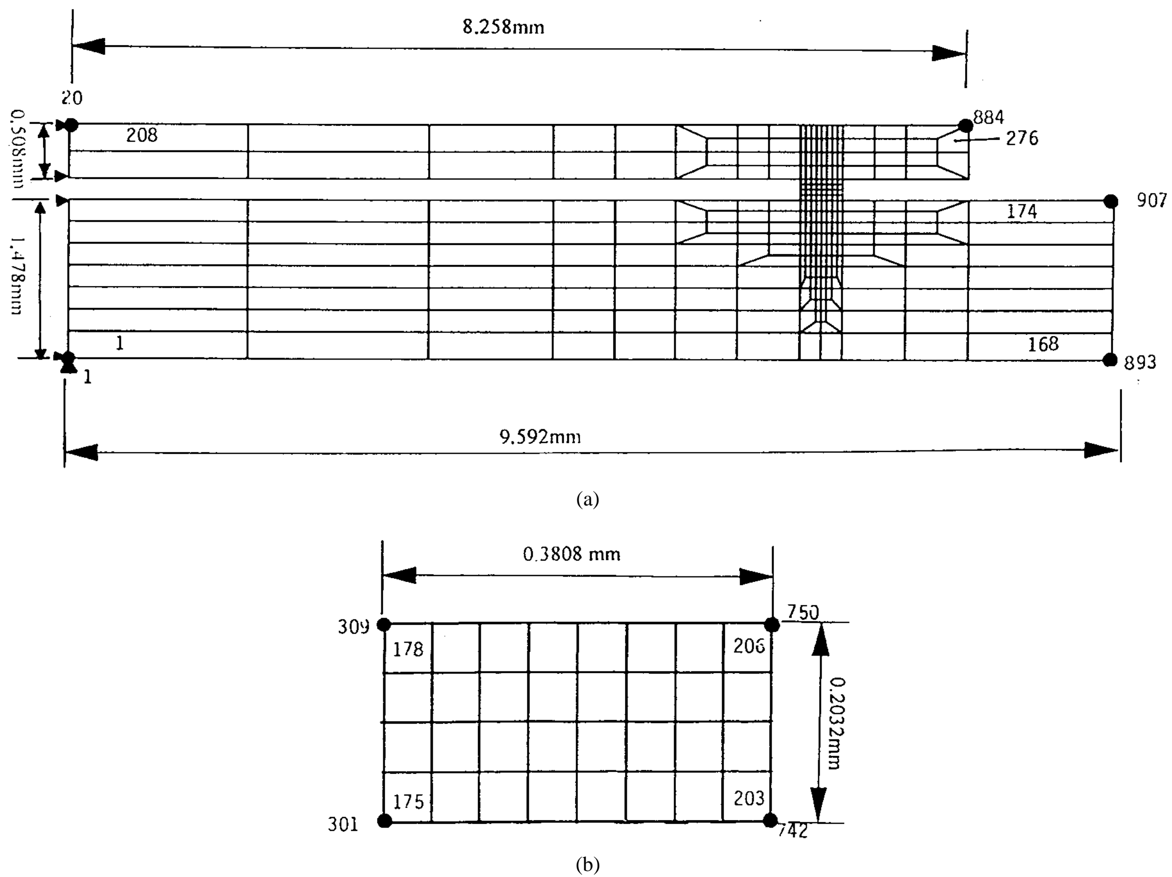

(a)

(b)

Fig. 5. Finite element meshes for LCCC: (a) chip-solder-PWB and (b) solder.

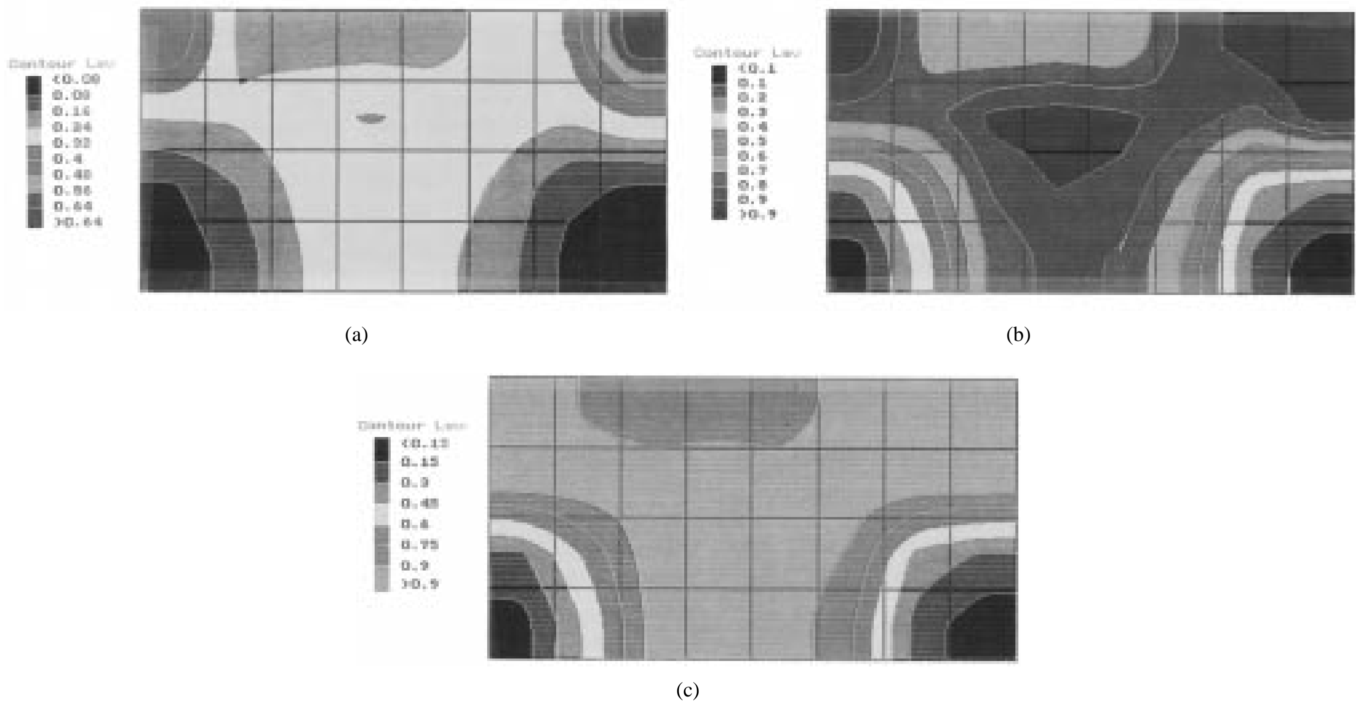

(a) (b)

(c)

Fig. 6. Distribution of disturbance in solder at different thermal cycles: (a) $N = 100$, (b) $N = 300$, and (c) $N = 400$.

It is simple to trace in the FE procedure. This is because it is a part of the constitutive model and its calculation with the nonlinear cyclic analysis is an integral part of the FE calculations. It has been shown [6], [7] that the critical disturbance criterion is consistent and relevant to the energy [25] and load-drop criteria [18] used previously. However, the procedure proposed here provides a general criterion based on multidimensional effects. Fig. 7 shows plots of disturbance

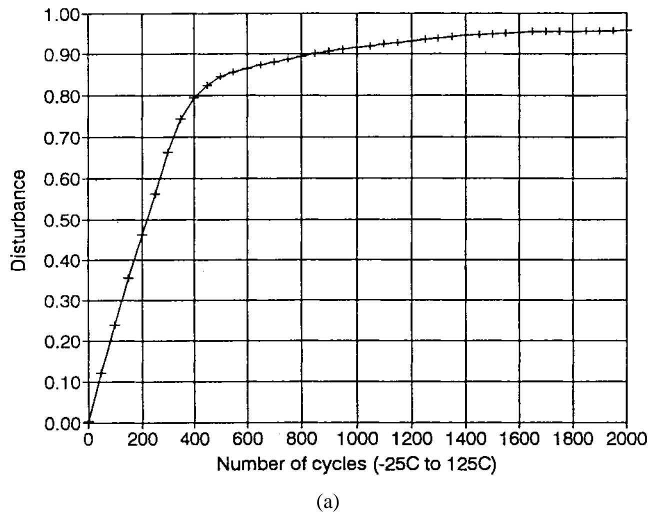

(a)

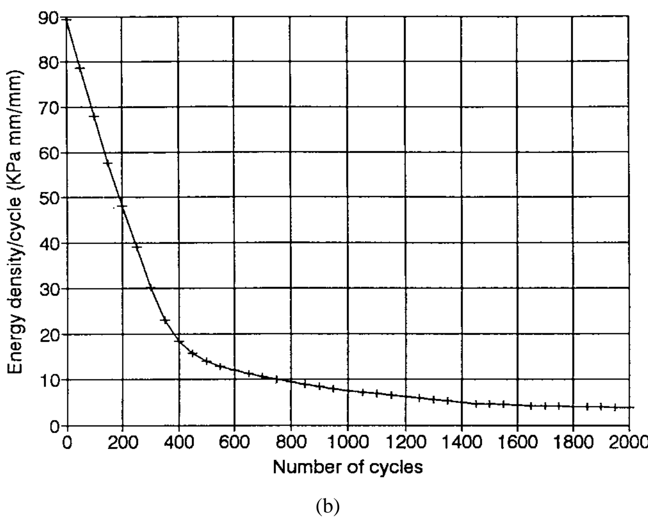

(b)

Fig. 7. Computed variation of disturbance and energy density per cycle with number of cycles: (a) D versus N and (b) energy/cycle.

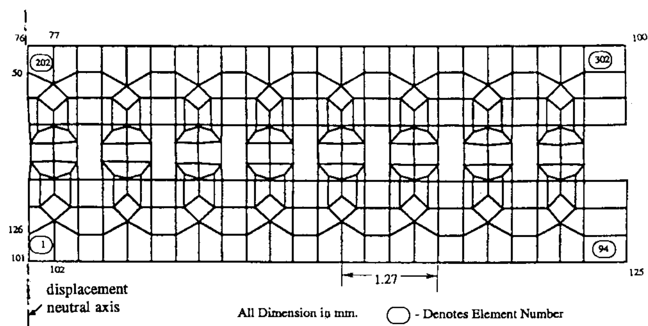

Fig. 8. Typical finite element mesh for ball spacing = 1.27 mm.

and energy density/cycle with number of cycles. At about 400 cycles, there occurs a significant change in D, and in the rate of change of energy leading to their stabilization and saturation, which corresponds to the almost complete failure, Fig. 6(c).

Example 2: Solder Ball Connect (SBC) Package: The SBC structure forms a second-level assembly in surface mount technology. Here, the solder ball is composed of (90% Pb-10% Sn) with (63% Pb-37% Sn) solder fillers. This

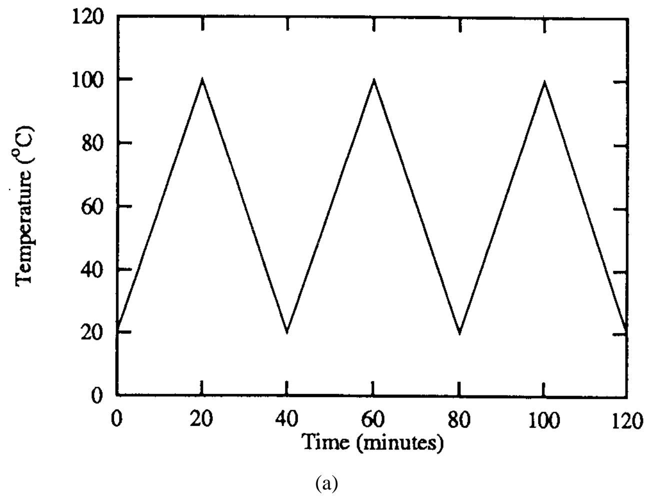

(a)

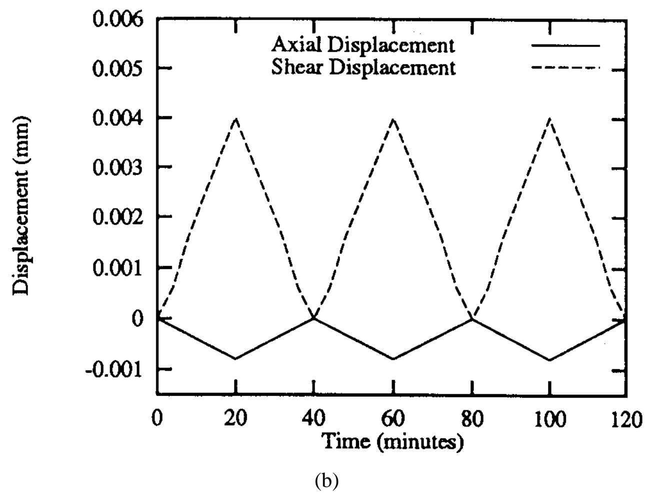

(b)

Fig. 9. Thermal cycles and applied displacements: (a) Thermal cycles and (b) axial and shear displacements from macromodel applied to micromodel for ball spacing = 1.27 mm.

problem was analyzed by Corbin [22] using a finite element procedure (ANSYS). In order to reduce computational effort, Corbin analyzed the problem by performing two level analyzes: macro and micro. The macro model simulated the ceramic module and the FR-4 card using thin plate elements connected by beam elements to simulate the SBC ball-joint structure. The ceramic module and FR-4 were assumed to be linear elastic, while the solders (90% Pb-10% Sn in the solder balls and 63% Sn-37% Pb in the solder fillers) were assumed to be elastoplastic with temperature-dependent elastic moduli (E and ν), and yield stress, σ_y. The net or relative (axial and shear) displacements from the macro analysis were then used as input boundary-loading conditions for the extreme ball, which was idealized as three-dimensional. Corbin compared the computer results with laboratory observations on SBC package using Laser Moire Interferometry reported by Guo *et al.* [24] (Fig. 4).

Present Analysis: The above problem was analyzed by using the proposed DSC model and the associated finite element procedure [7], [8]. There are differences between the analysis by Corbin and the present analysis.

1) In the present analysis, the behavior of the solders is simulated by using the DSC model which allows plas-

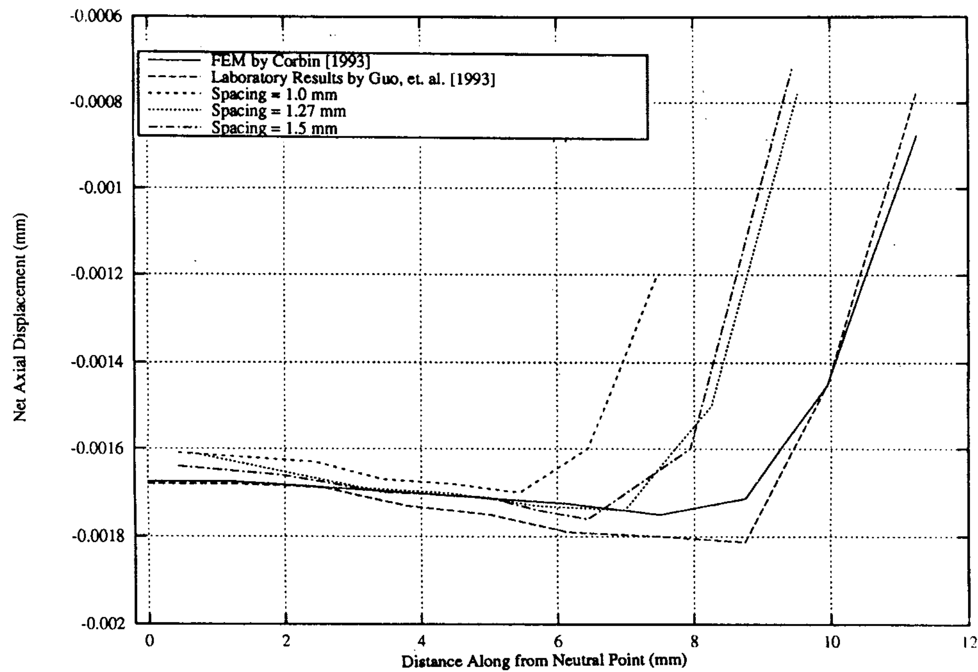

(a)

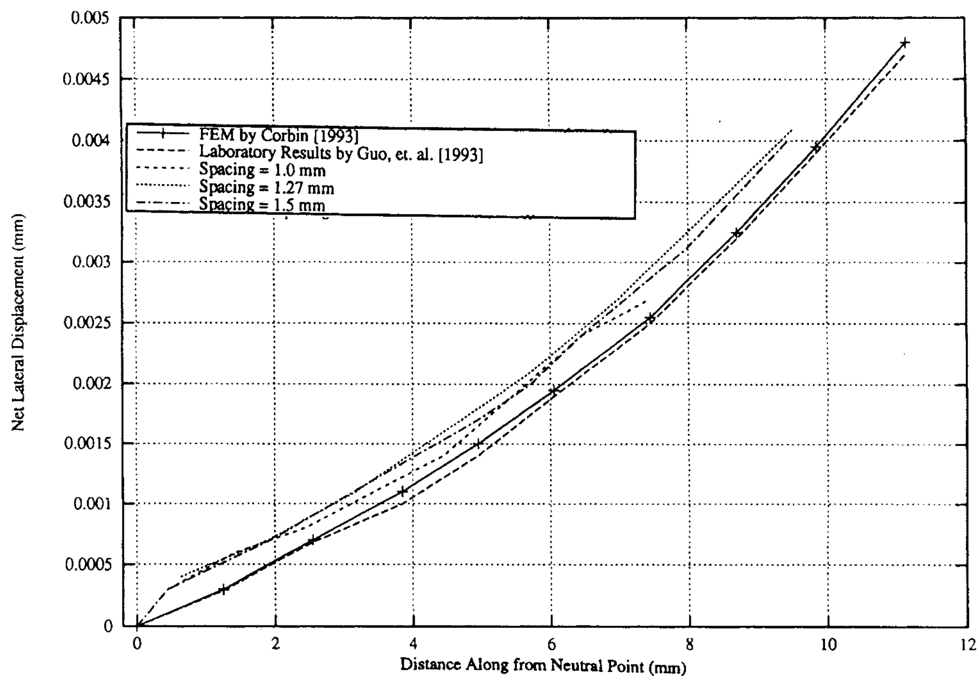

(b)

Fig. 10. Computed displacements and comparisons with previous FE analysis [22] and test data [24]: (a) axial displacement and (b) shear displacement.

tic yielding, and disturbance which allows for internal microcracking and resulting degradation of the strength of the solders.

2) The dimensions of the module/ball-arrays/card system are somewhat different. Corbin [22] considered a 25 $\times$ 25 mm SBC module, which represented one-quarter of a 19 $\times$ 19 array of solder balls spaced 1.27 mm apart (center to center). In the present analysis the structure analyzed was smaller, 21 $\times$ 21 mm, as reported in [23]. Also, the present study includes a parametric evaluation of the effect of different solder ball spacings (1.00, 1.27, and 1.5 mm) on the response of the system.

3) In the present analysis, the FE procedure used is two-dimensional plane strain idealization. However, to reduce computational effort, the analysis was performed using two levels, macro and micro. In the macro level, half of the structure was idealized; Fig. 8 shows the FE mesh with 4-node elements for typical solder ball spacing of 1.27 mm, with 360/304 nodes/elements. The IBM RS/6000 computer at Cornell Theory Center was

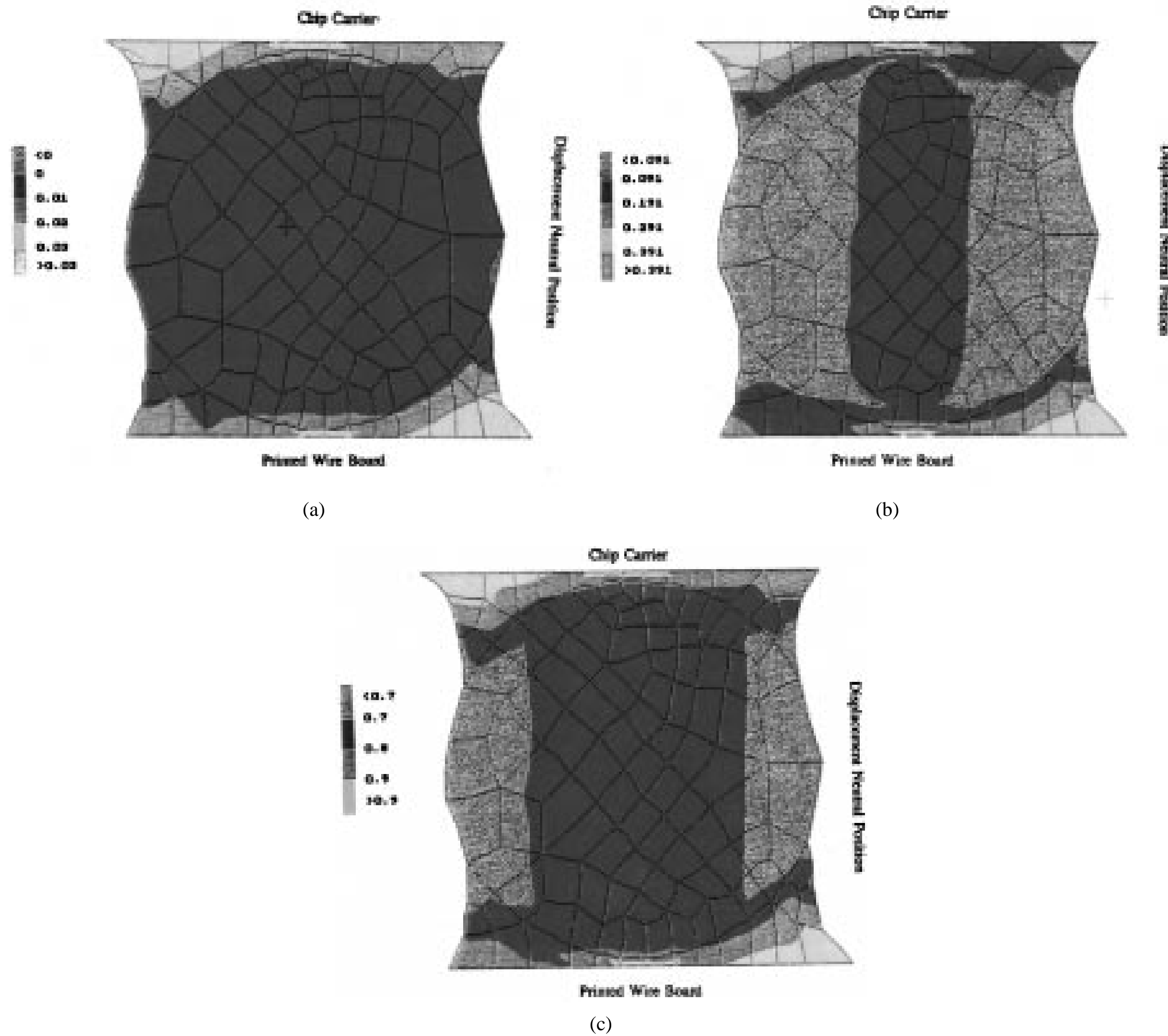

Fig. 11. Distribution of disturbance in solder ball for 1.27 mm spacing at different thermal cycles: (a) $N = 100$, (b) $N = 500$, and (c) $N = 873$.

used for the FE calculations. Then the results from the macro model were used to perform detailed analysis at the micro level which involved single solder ball; the FE mesh for typical ball spacing is indicated in the subsequent Fig. 11.

4) The molybdenum and copper pads at the top and bottom of the ball are not included in this analysis. This is done to simplify the analysis, and also because failure is often initiated in the filler and not in the pads.

Details: In the macrolevel, the system was subjected to a single (first) thermal cycle, Fig. 9(a). The resulting shear (translation) and normal (axial) displacements were computed for application at the mid-plane of the extreme solder ball; typical results for the ball spacing of 1.27 mm are shown in Fig. 9(b).

Fig. 10 shows computed axial (normal) and shear displacements from the macro model, which were applied to the single ball in a number of thermal cycles for $N = 1000$. It is recognized that the displacement amplitudes would change (increase) with thermal cycles due to plastic deformations and microcracking with cycles. However, in order to reduce computational effort required for performing the macrolevel analysis for all cycles, and as a simplification, the amplitudes determined from the first thermal cycle were used for all thermal cycles in the micromodel.

Analysis of Results: Fig. 10 shows computed axial and shear displacements for different ball spacings. Finite element results obtained by Corbin [22] and experimental data from Guo [24] are also shown for comparison. The present analysis shows satisfactory correlation with the test data. A part of the difference can be due to the fact that the size of the module [23] analyzed here is smaller than that used by Corbin and in the laboratory tests. Also, the displacements from the present analysis are greater partly because the effect of disturbance (microcracking) is included in the DSC model used. Furthermore, the present analysis is two-dimensional, whereas Corbin [22] used three-dimensional analysis for the ball. Fig. 10 shows that the displacements are smaller for smaller via spacings. However, as the spacing increases, it appears that the differences in displacements at higher spacing tend to diminish.

Disturbance growth and localization with thermal cycles were computed for the three ball spacings. However, in view

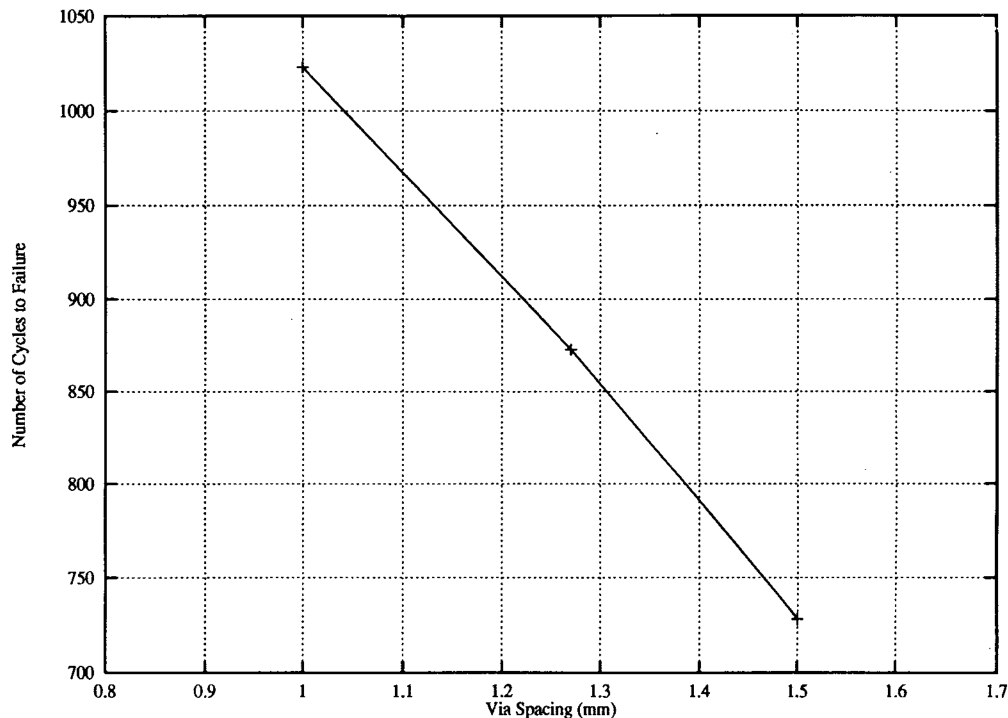

Fig. 12. Plot of the number of cycles to failure versus via spacing for three ball spacings.

of the space limitations, only typical distributions for the ball spacing of 1.27 mm at $N = 100$, 500, and $N_f = 873$ are included in Fig. 11. The localization of disturbance initiates near the top left and bottom right corners of the ball and propagates with cycles; this localization grows along the filler. Note that the displacement neutral axis in Fig. 11 on the right side is reversed. The trends of the growth of disturbance and localization compare well with that of strains reported by Guo [24] and Corbin [22]. It is assumed that the critical disturbance $D_c = 0.90$. Fig. 11 shows that at about $N_f = 873$ for the 1.27 mm spacing, the growth of D_c has extended to the major part, about 80 to 90% width of the ball. A plot of number of cycles at failure, N_f, versus ball spacing is shown in Fig. 12; it can be seen that the values of N_f decrease as the spacing increases. In other words, a package with a smaller ball spacing can sustain greater number of thermal cycles. Similar and additional research can lead to reliability and optimized analyzes as affected by significant design factors. The present analysis for SBC does not include creep effects. Notwithstanding this, the analysis from the elastoplastic with disturbance characterization for the solders, the results yield satisfactory prediction of the thermomechanical response of the SBC package.

VI. Conclusion

The disturbed state concept can provide a unified and integrated approach for constitutive modeling of thermomechanical behavior of materials and joints in electronic packaging problems. Its hierarchical nature allows the user to choose simple to sophisticated models for specific material and need. Various versions of the model have been calibrated based on available laboratory tests for different Pb-Sn solders and ceramic chip materials. The DSC model is implemented in a nonlinear finite element (FE) procedure that allows a wide range of models, elastic, thermoplastic, and thermoviscoplastic with disturbance. The FE procedure is used to analyze two problems in electronic packaging: Leadless Ceramic Chip Carrier, and Solder Ball Connect package. Here, results from the thermoviscoplastic and thermoplastic analysis with disturbance (microcracking and degradation) are compared with experimental data and a previous finite element analysis. The results permit evaluation of stresses, strains and disturbance with cyclic thermal loading. Identification of growth of disturbance with cycles permits tracing of microcracking and fatigue failure based on the critical disturbance. This can lead to design and reliability analysis in electronic packaging.

Acknowledgment

The authors would like to thank Dr. T. Kundu, CEEM Department, University of Arizona, Tucson, Dr. D. Frear, Sandia National Laboratory, Albuquerque, NM, Dr. E. Suhir, AT&T Bell Labs, Murray Hill, NJ, and Dr. M. Cole, IBM Research Center, Hopewell Junction, NY, for their assistance and input.

References

[1] R. Tummula and E. Rynaszewski, Eds., *Microelectronics Packaging Handbook*. New York: Van Nostrand Reinhold, 1989.
[2] M. Pecht, *Handbook of Electronic Package Design*. New York: Marcel Dekker, 1988.
[3] E. Suhir, "Analytical modeling in electronic packaging structures: Its merits, shortcomings and interaction with experimental and numerical techniques," *J. Electron. Packag.*, vol. 111, pp. 157–161, 1989.
[4] J. H. Lau, Ed., *Solder Joint Reliability Theory and Applications*. New York: Van Nostrand Reinhold, 1991.

[5] D. R. Frear, S. N. Burchett, H. S. Morgan, and J. H. Lau, Eds., *The Mechanics of Solder Alloy Interconnects*. New York: Van Nostrand, 1994.
[6] C. S. Desai, J. Chia, T. Kundu, and J. L. Prince, "Thermomechanical response of materials and interfaces in electronic packaging: Part I—Unified constitutive models and calibration, Part II—Unified constitutive models, validation and design," *ASME J. Electron. Packag.*, vol. 119, pp. 294–309, Dec. 1997.
[7] C. Basaran, C. S. Desai, and T. Kundu, "Thermomechanical finite element analysis of problems in electronic packaging using the disturbed state concept, Part I: Theory and formulations, Part II: Verification and applications," *ASME J. Electron. Packag.*, Feb. 1998.
[8] T. Dishongh and C. S. Desai, "Disturbed state concept for materials and interfaces with applications in electronic packaging," Rep. NSF, Dept. of Civil Eng. Eng.. Mech., The University of Arizona, Tucson, AZ, 1996.
[9] C. S. Desai, "Constitutive modeling using the disturbed state as microstructure self-adjustment concept," in *Continuum Models for Materials with Microstructure*, H. P. Mühlhaus, Ed. London, U.K.: Wiley, 1995, ch. 8.
[10] C. S. Desai and J. Toth, "Disturbed state constitutive modeling based on stress-strain and nondestructive behavior," *Int. J. Solids Struc.*, vol. 33, no. 11, pp. 1619–1650, 1996.
[11] L. M. Kachanov, *Introduction to Continuum Damage Mechanics*. Dordrecht, The Netherlands: Martinus Nijhoff, 1986.
[12] K. H. Roscoe, A. Schofield, and C. P. Wroth, "On the yielding of soils," *Geotechnique*, vol. 108, pp. 22–53, 1958.
[13] H. S. Riemer, "Prediction of temperature cycling life for SMT solder joints on TCE-mismatched substances," in *Proc. IEEE Electron. Comp.*, 1990, pp. 418–423.
[14] N. Nir, T. D. Duddear, C. C. Wang, and A. R. Storm, "Fatigue properties of microelectronic solder joints," *ASME J. Electron. Packag.*, vol. 113, 1991.
[15] M. Cole, T. Caufield, D. Banks, M. Winton, A. Walsh, and S. Gonya, "Constant strain rate tensile properties of various lead based solder alloys at 0, 50 and 100 °C," in *Proc. Microelectron. Packag. Conf.*, Montreal, P.Q., Canada, 1991.
[16] T.-Y. Pan, "Thermal cyclic induced plastic deformations in solder joints—Part I: Accumulated deformation in surface mount joints," *Trans. ASME*, vol. 113, pp. 8–15, 1991.
[17] A. Skipor, S. Harren, and J. Bostis, "Constitutive characterization of 63/37 Sn/Pb eutectic solder using the Bodner-Parton unified creep-plasticity model," in *Proc. Joint ASME/JSME Conf. Electron. Packag.*, W. T. Chen and H. Abe, Eds., 1992, vol. 2, pp. 661–672.
[18] H. D. Solomon, "Isothermal fatigue of LCC/PWB interconnections," *ASME J. Electron. Packag.*, vol. 114, pp. 161–168, 1992.
[19] E. Savage and G. Getzan, "Mechanical behavior of 60 tin/40 lead solder at various strain rates and temperatures," in *Proc. Int. Soc. Hybrid Microelectron. (ISHM)*, Nashville, TN, 1990.
[20] P. Perzyna, "Fundamental problems in viscoplasticity," in *Advances in Applied Mechanics*. New York: Academic, 1996, pp. 244–368.
[21] P. M. Hall and W. M. Sherry, "Materials, structures and mechanics of joints for surface-mount microelectronic technology," in *Proc. 3rd Int. Conf. Techniques de Connexion en Electronique*, Welding Soc., Fellbach, Germany, 1986, pp. 18–20.
[22] J. S. Corbin, "Finite element analysis for solder ball connect (SBC) structural design optimization," *IBM J. Res. Develop.*, vol. 37, no. 5, pp. 585–596, 1993.
[23] IBM, "CBGA and CCGA module limitations, inspection, and specifications," IBM Doc. 67F4333, Oct. 1995.
[24] Y. Guo, C. K. Lim, W. T. Chen, and C. G. Woychik, "Solder ball connect (SBC) assemblies under thermal loading: I. Deformation measurements via Moiré interferometry and its interpretation," *IBM J. Res. Develop.*, vol. 37, no. 5, pp. 635–647, 1993.
[25] A. Dasgupta, C. Oyan, D. Barker, and M. Pecht, "Solder creep-fatigue analysis by an energy-partitioning approach," *ASME J. Electron. Packag.*, vol. 114, 1992.

Chandra S. Desai received the B.S. degree from the University of Bombay, Bombay, India, the M.S. degree from Rice University, Houston, TX, and the Ph.D. degree from the University of Texas at Austin.

Currently, he is a Regents' Professor and Director for Center for Material Modeling and Computational Mechanics, Department of Civil Engineering and Engineering Mechanics, The University of Arizona, Tucson. He is involved in analytical and experimental research in constitutive modeling for a wide range of materials, and computational methods for problems in civil and mechanical engineering, and electronic packaging. He is author/coauthor/editor of 17 books and over 250 papers.

Cemalettin Basaran received the M.S. degree from the Massachusetts Institute of Technology, Cambridge, and the Ph.D. degree from The University of Arizona, Tucson.

He is an Assistant Professor in the Department of Civil Engineering, State University of New York at Buffalo. His main research area is experimental and numerical study of response of power electronics packaging subjected to concurrent thermal cycling, and dynamic loading.

Dr. Basaran received the Department of Defense ONR Young Investigator Award in 1997.

Terrance Dishongh received the B.S. and M.S. degrees, both in engineering mechanics, from the University of Tennessee, Knoxville, and the Ph.D. degree from The University of Arizona, Tucson, in 1966.

He completed his post-doctoral work at the University of Maryland, College Park, in the CALCE-Electronic Packaging Research Center. He is now with Intel Corporation, Hillsboro, OR.

John L. Prince (S'65–M'68–SM'78–F'90) received the B.S.E.E. degree from Southern Methodist University, Dallas, TX, and as an NSF Graduate Fellow received the M.S.E.E. and Ph.D. degrees in electrical engineering from North Carolina State University, Raleigh.

He is currently Professor of Electrical and Computer Engineering and Director of the Center for Electronic Packaging Research at The University of Arizona, Tucson. He came to The University of Arizona in 1983. He has been Principal Investigator of the Semiconductor Research Corporation (SRC) Program in VLSI Packaging and Interconnection Research at the university since 1984. He has extensive industrial experience, including silicon device, circuit, and reliability work at Texas Instruments from 1970 to 1975, silicon research at the Research Triangle from 1968 to 1970, and medical device design and reliability at Intermedics, Inc., from 1980 to 1983. His current research interests center on developing modeling and simulation techniques for switching noise in packages and MCM's, on modeling and simulation techniques for mixed-signal system packaging, and on developing high frequency measurements on packaging structures. His is author or co-author of 140 papers in the field of packaging, and 30 papers in the fields of device physics, process development, and reliability.